

Investigation of proton spin relaxation in water with dispersed silicon nanoparticles for potential magnetic resonance imaging applications

Yu. V. Kargina, M. B. Gongalsky, A. M. Perepukhov, A. A. Gippius, A. A. Minnekhanov, E. A. Zvereva, A. V. Maximychev, and V. Yu. Timoshenko

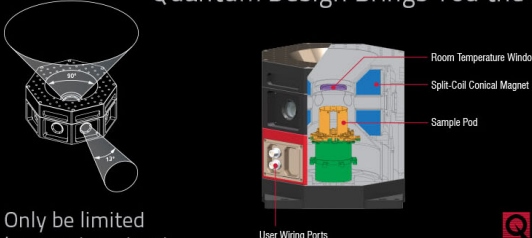
Citation: *Journal of Applied Physics* **123**, 104302 (2018); doi: 10.1063/1.5006846

View online: <https://doi.org/10.1063/1.5006846>

View Table of Contents: <http://aip.scitation.org/toc/jap/123/10>

Published by the [American Institute of Physics](#)

Quantum Design Brings You the Next Generation Magneto-Optic Cryostat



Only be limited by your imagination...

8 Optical Access Ports: 7 Side; 1 Top
Temperature Range: 1.7 K to 350 K
7 T Split-Coil Conical Magnet
Low Vibration: <10 nm peak-to-peak
89 mm x 84 mm Sample Volume
Automated Temperature & Magnet Control
Cryogen Free

Quantum Design
qdusa.com/opticool5



Investigation of proton spin relaxation in water with dispersed silicon nanoparticles for potential magnetic resonance imaging applications

Yu. V. Kargina,^{1,2,a)} M. B. Gongalsky,¹ A. M. Perepukhov,³ A. A. Gippius,^{1,4}
 A. A. Minnekhanov,¹ E. A. Zvereva,^{1,5} A. V. Maximychev,³ and V. Yu. Timoshenko^{1,2,6}

¹Faculty of Physics, Lomonosov Moscow State University, 119991 Moscow, Russia

²National Research Nuclear University "MEPhI," Phys-Bio Institute, Laboratory of BioNanoPhotonics, 115409 Moscow, Russia

³Moscow Institute of Physics and Technology, 141700 Dolgoprudny, Moscow Region, Russia

⁴Shubnikov Institute of Crystallography, 119333 Moscow, Russia

⁵National Research South Ural State University, 454080 Chelyabinsk, Russia

⁶Lebedev Physical Institute of RAS, 119333 Moscow, Russia

(Received 28 September 2017; accepted 24 February 2018; published online 12 March 2018)

Porous and nonporous silicon (Si) nanoparticles (NPs) prepared by ball-milling of electrochemically etched porous Si layers and crystalline Si wafers were studied as potential agents for enhancement of the proton spin relaxation in aqueous media. While nonporous Si NPs did not significantly influence the spin relaxation, the porous ones resulted in strong shortening of the transverse relaxation times. In order to investigate an effect of the electron spin density in porous Si NPs on the proton spin relaxation, we use thermal annealing of the NPs in vacuum or in air. The transverse relaxation rate of about 0.5 l/(g s) was achieved for microporous Si NPs, which were thermally annealing in vacuum to obtain the electron spin density of the order of 10^{17} g^{-1} . The transverse relaxation rate was found to be almost proportional to the concentration of porous Si NPs in the range from 0.1 to 20 g/l. The obtained results are discussed in view of possible biomedical applications of Si NPs as contrast agents for magnetic resonance imaging. *Published by AIP Publishing.*

<https://doi.org/10.1063/1.5006846>

I. INTRODUCTION

Magnetic resonance imaging (MRI) is a powerful biomedical diagnostics method, which is usually tuned on nuclear magnetic resonance of hydrogen atoms (protons). The contrast for MRI is known to be provided by changes of the longitudinal (T_1) and transverse (T_2) times of the proton spin relaxation. In order to improve the contrast, several intravenously administered contrast agents (CA) such as paramagnetic ions, e.g., Gd^{3+} , Fe^{3+} , Mn^{3+} , are used.^{1–6} CAs change the MRI signal of an investigated area by changing the relaxation times of the nearby protons. The most widespread CAs available for clinical use are Gd-based ones. However, Gd^{3+} ions can cause nephrogenic systemic fibrosis and can also prevent calcium-ion passage through muscle cells that block the flow of calcium in bone epiphyses.^{2–5} Superparamagnetic NPs of iron oxide (SPIO) demonstrate the enhancement of the T_2 -weighted MRI contrast, but their toxicity still remains significant.⁶

Silicon (Si) nanoparticles (NPs) are promising for biomedical applications. There are many *in vitro* studies of the toxicity of Si NPs which reveal the low level of their toxicity and biodegradability.^{7–9} *In vitro* toxicity of Si NPs was evaluated by various well-known approaches including: (i) MTT and calcein assays showed complete absence of the cytotoxicity for the concentrations up to 0.2 mg/ml,⁷ (ii) flow cytometry showed negligible cytotoxicity and low apoptotic

activity for concentration of microporous Si (μPSi) NPs about 0.1 mg/ml,⁸ (iii) impedance-based growth control (xCELLigence) showed stable cell growth rate up to 1 mg/ml.⁹ While *in vivo* studies of the toxicity of silica (SiO_2) based NPs were performed, the *in vivo* studies of safety profiles of silicon (Si) based NPs are not yet completed. However, several papers were devoted to the *in vivo* studies of porous Si NPs toxicity. Si NPs were injected intraperitoneally to the mice which caused no genotoxicity and reproductive toxicity up to 50 mg/kg according to DNA comet assay in contrast to silica nanoparticles.^{10–12} Porous Si NPs (20 mg/kg) were injected intravenously into mice and it was shown that mice continue to mature without any significant toxic effects.⁷ Intravenous tail vein injection of dextran covered porous Si NPs of a dose of 30 mg/kg was found to be almost nontoxic.¹³ Additionally, Si NPs can dissolve in aqueous media by forming orthosilicic acid $\text{Si}(\text{OH})_4$, which is withdrawn from the body.^{7,14} Si NPs may be coated with biocompatible polymers that protect them from rapid dissolution and reduce their toxicity.^{9,13,15}

Si NPs can provide therapeutic modalities acting as photosensitizers,¹⁶ sonosensitizers,^{13,17} and radiofrequency radiation-induced hyperthermia sensitizers.¹⁸ Si NPs have also been shown to be hyperpolarized MRI agents.¹⁹ Si NPs with incorporated Gd^{3+} ions were proposed as CAs for MRI.²⁰

Recently, we have shown that porous Si NPs themselves could act as efficient CAs for MRI in phantom experiments.²¹ The most probable explanation of the contrast property of porous Si NPs is based on a hypothesis of the magnetic dipole–dipole interaction between electron spins on the surfaces of the NPs and surrounding protons (see Fig. 1). While a solid

^{a)}Author to whom correspondence should be addressed: juliakargina@gmail.com

NP itself can be a sensitizer of the proton spin relaxation [see Fig. 1(a)] as it was discussed in Ref. 22, porous Si NPs provide additional opportunities to increase the spin center density [see Fig. 1(b)] due to both the pore morphology and surface treatments. Indeed, porous Si usually contains a lot of paramagnetic centers as unpaired (dangling) Si bonds and the center number can be significantly modified by physical and chemical treatments.²³ In this paper, we investigate aqueous suspensions of Si NPs prepared from mesoporous, microporous, and nonporous crystalline silicon in order to reveal the role of paramagnetic centers in NPs for the proton spin relaxation and to find a possible way to improve the CA properties of Si NPs for MRI applications.

II. EXPERIMENTAL

Porous silicon (PSi) films were formed by the electrochemical etching of (100)-oriented c-Si wafers in a solution based on hydrofluoric acid and ethanol [HF(49%):C₂H₅OH = 1:1] (see, for example, reviews^{23,24}). In order to remove the surface oxide, c-Si wafers had been preliminarily dipped into a 5 M HF solution. Mesoporous Si (MPSi) were produced by etching of p-type heavily boron-doped wafer with specific resistivity of 25 mΩ cm for 60 min under 60 mA/cm² current density. Samples of microporous Si (μ PSi) were prepared from lightly boron-doped (100)-oriented c-Si wafers with specific resistivity of 10–20 Ω cm and etching time of 30 min. The prepared PSi films were lifted off by a short increase of the current density up to 500–600 mA/cm². NPs were prepared by grinding of the PSi films in deionized water in a “FRITSCH Pulverisette 7 premium line” planetary-type mill for 30 min. The concentration of NPs in suspensions was determined by a gravimetric method and it was about 25 g/l for as-prepared samples. The suspensions were diluted by pure water to obtain the NP concentrations in the range from 0.1 to 22 g/l for further experiments. Nonporous crystalline Si nanoparticles (c-Si NPs) were prepared by milling (100)-oriented p-type heavily boron-doped c-Si wafers with specific resistivity of 10–25 mΩ cm in deionized water for 30 min.

The structural properties of Si NPs were investigated by using a LEO912 AB OMEGA transmission electron microscope (TEM). TEM images were additionally obtained with negative staining of porous Si NPs by phosphotungstic acid. Sizes and zeta-potentials of the prepared Si NPs in water

solutions were studied by means of dynamic light scattering (DLS) with a Malvern Zetasizer Nano ZS. Prior DLS measurements, the NP suspensions were additionally diluted by water to the concentration of 0.01 g/l to ensure lowering optical losses, and avoid multiphoton scattering and NPs agglomeration.

The surface composition of Si NPs was analyzed with a Bruker IFS 66v/S Fourier-transform infrared (FTIR) spectrometer. The FTIR transmission spectra were measured for dried NPs deposited on double-side optically polished c-Si wafers (lightly boron-doped, specific resistivity 10–20 Ω cm). Electron paramagnetic resonance (EPR) spectra of dried Si NPs were measured at room temperature by using a Bruker EPR spectrometer ELEXSYS-500 ($f \approx 9.4$ GHz, $B \leq 1.4$ T) and an EPR spectrometer CMS 8400 ADANI ($f \approx 9.4$ GHz, $B \leq 0.7$ T). The effective g -factors of samples have been calculated with respect to a reference sample of BDPA (a,g-bis-diphenyl-*b*-phenylallyl) with g -factor 2.00359. To estimate the concentration of paramagnetic centers from EPR data, the reference sample of CuCl₂·2H₂O has been used. The relaxation times T_1 and T_2 were measured by a Bruker Minispec NMR Relaxometer with 20 MHz probe and magnetic field 0.5 T at 40 °C.

III. RESULTS AND DISCUSSION

Figure 2 shows typical TEM images of the investigated NPs of c-Si, MPSi, and μ PSi. One can see that c-Si NPs consist of monocrystalline grains with typical sizes 100–200 nm [see Fig. 2(a)]. MPSi and μ PSi NPs reveal porous morphology with minimal sizes of Si nanocrystals about 10–20 nm, which are agglomerated into larger NPs with sizes above 100 nm [see Figs. 2(b) and 2(c)]. The corresponding electron diffraction patterns [insets in Figs. 2(b) and 2(c)] indicate that the porous NPs are composed of randomly oriented Si nanocrystals. TEM images of the stained porous NPs give additional evidences on their porous morphology and sizes (see Fig. 1 in supplementary material).

According to DLS data, the most probable size (hydrodynamic diameter) of μ PSi NPs is 60 nm, while a broad shoulder of the size distribution in the region from 100 to 200 nm is present [see Fig. 3(a)]. NPs of MPSi and c-Si are characterized by the mean size about 100 nm and broad tails of the size distribution till 300–400 nm. Zeta-potentials of all investigated NPs were found to be about –25...–45 mV, which are typical for Si NPs. The relatively large absolute value of the zeta-potential prevents NPs from agglomeration and thereby stabilizes suspension characteristics.

Figure 3(b) shows FTIR transmittance spectra of the prepared NPs after deposition on c-Si substrates and drying in air. The FTIR spectra reveal a strong absorption band in the region of 1000...1200 cm⁻¹ related to the Si-O-Si bond vibrations that indicates the silicon oxide coating of NPs.

Typical transients of the longitudinal and transverse proton magnetization of pure water and aqueous suspensions of NPs are shown in Fig. 4. One can see that the longitudinal magnetization [Fig. 4(a)] is less sensitive to the presence of NPs than the transverse one [Fig. 4(b)] and the both

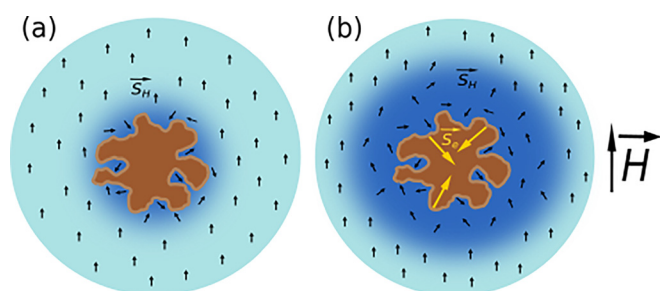


FIG. 1. (a) Schematic view of the shortening of proton spin relaxation in water (blue regions) nearby the NP (brown spot) without unpaired electron spins; (b) the same scheme for the NP with a number of unpaired electron spins. Black and yellow arrows correspond to the proton and electron spins, respectively.

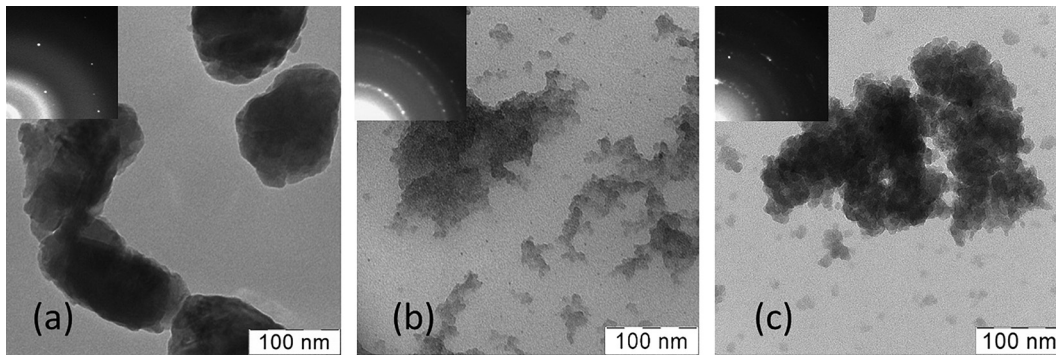


FIG. 2. TEM images of NPs prepared from (a) c-Si, (b) MPSi, and (c) μ PSi. Insets show fragments of the corresponding electron diffraction patterns.

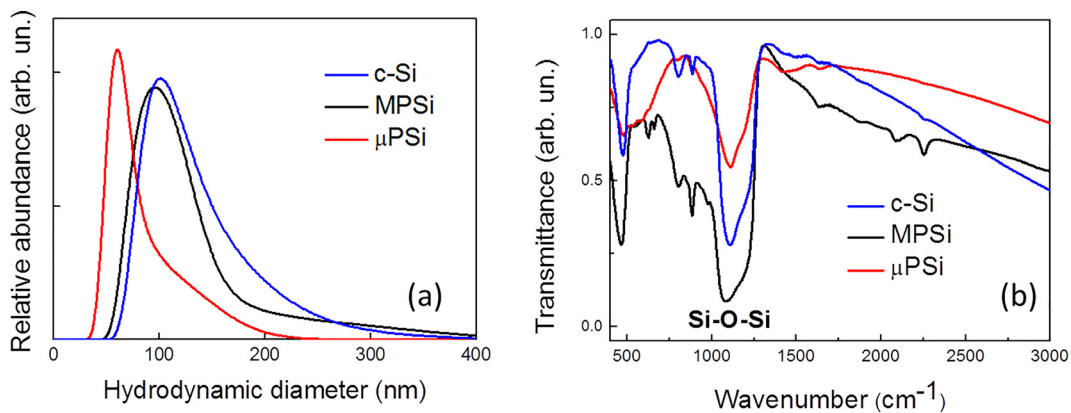


FIG. 3. (a) DLS spectra of diluted aqueous suspensions of NPs prepared from c-Si (blue line) MPSi (black line) and μ PSi (red line); (b) FTIR spectra of the corresponding dried NPs.

transients reveal faster and slower decay times in the case of μ PSi NPs and c-Si ones, respectively. The corresponding T_1 and T_2 times for the suspensions with NP concentration of 1 g/l are shown in Table I.

The observed shortening of the relaxation times can be related to the effect of paramagnetic centers on the surfaces of NPs as it is schematically shown in Fig. 1. PSi NPs obtained by electrochemical etching contain a large number of paramagnetic centers as Si dangling bonds (DBs), which were detected by EPR spectroscopy and the corresponding numbers are given in Table I.

Several types of Si DBs, e.g., P_{b0} and P_{b1} centers, where P_{b0} centers are DBs on the (111) and (100) Si/SiO₂ surface interface,^{25–28} can contribute to the total density of paramagnetic centers in the investigated NPs. Although c-Si NPs possess a valuable number of Si DBs $\sim 10^{16} \text{ g}^{-1}$, they did not induce significant shortening of the proton relaxation times (see Table I). It can be related to the nonporous morphology of c-Si NPs that determines their relatively low surface area. The shortening of T_2 is stronger for μ PSi NPs than for MPSi ones and this fact can be explained by the larger number of Si DBs in the former (see Table I). Note, the difference in

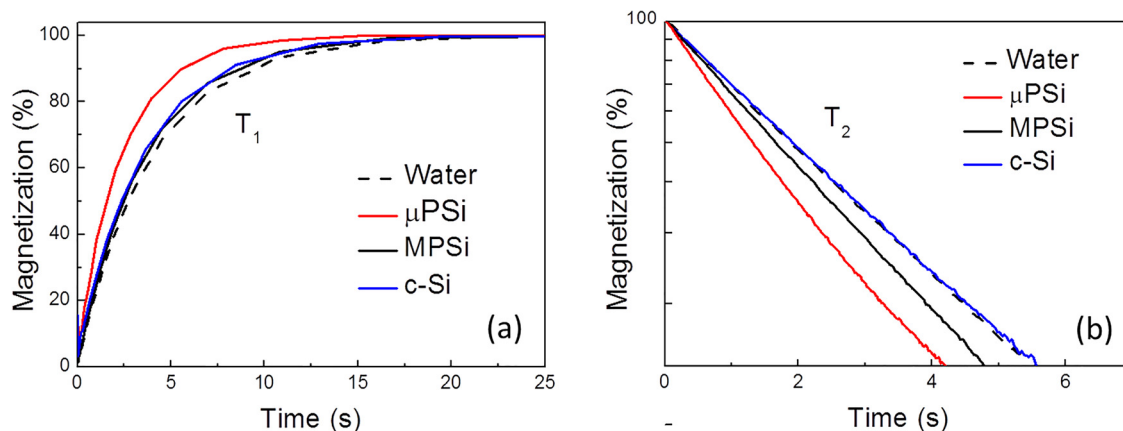


FIG. 4. Transients of (a) longitudinal and (b) transverse proton magnetization of pure water (black dashed line) and aqueous suspensions of NPs (with concentration of 1 g/l) prepared from c-Si (blue line) MPSi (black line) and μ PSi (red line).

TABLE I. Electron spin concentration in dried NPs, T_1 , and T_2 times for aqueous suspensions of NPs (concentration of 1 g/l) and those for pure water, for comparison.

Sample	Paramagnetic center concentration (1/g)	Proton relaxation times (s)	
		T_1	T_2
Crystalline Si (c-Si) NPs	2×10^{16}	3.6 ± 0.2	2.7 ± 0.2
Thermally oxidized meso porous Si (TO MPSi) NPs	3×10^{14}	3.5 ± 0.2	2.5 ± 0.2
Meso porous Si (MPSi) NPs	10^{15}	3.6 ± 0.2	2.3 ± 0.2
Micro porous Si (μ PSi) NPs	10^{16}	3.1 ± 0.2	1.7 ± 0.2
Micro porous Si NPs after thermal annealing (TA) in vacuum (TA μ PSi)	10^{17}	2.7 ± 0.2	1.2 ± 0.2
Water	0	4.0 ± 0.1	2.7 ± 0.1

pore sizes of μ PSi (≤ 2 nm) and MPSi (2–50 nm),²³ which determines different specific surface area, can also influence the interaction of water molecules with Si NDs on the surface of NPs.

In order to investigate the role of Si DB concentration in μ PSi NPs, we have performed their thermal annealing (TA) in vacuum with residual pressure of 10^{-3} Torr at 380°C for 2 h (TA μ PSi NPs). It is well known that the surface of as-prepared porous Si is passivated by hydrogen atoms.²³ During the heating in vacuum, the hydrogen coating is desorbed from the surface and new Si DBs can be formed.²⁵ Figure 5(a) shows EPR spectra of μ PSi NPs before and after TA treatment. The EPR spectrum of as-prepared μ PSi NPs is characterized by effective g-factor of about 2.005, which can be related to a superposition of different types of Pb centers.^{29,30} The TA μ PSi NPs resulted in an increase in the EPR intensity by 10 times and the spectrum became more symmetric [red curve in Fig. 5(a)]. The measurement of the relaxation times showed that the TA in vacuum resulted in shortening of the transverse times from 1.7 s to 1.2 s [see Fig. 5(b)]. Although the concentration of Si DBs (N_s) increased by 10 times (from 10^{16} to 10^{17} g $^{-1}$), the shortening of the relaxation times decreased only 3 times. The reason for that is partial passivation of the DBs on NPs surface by water molecules.

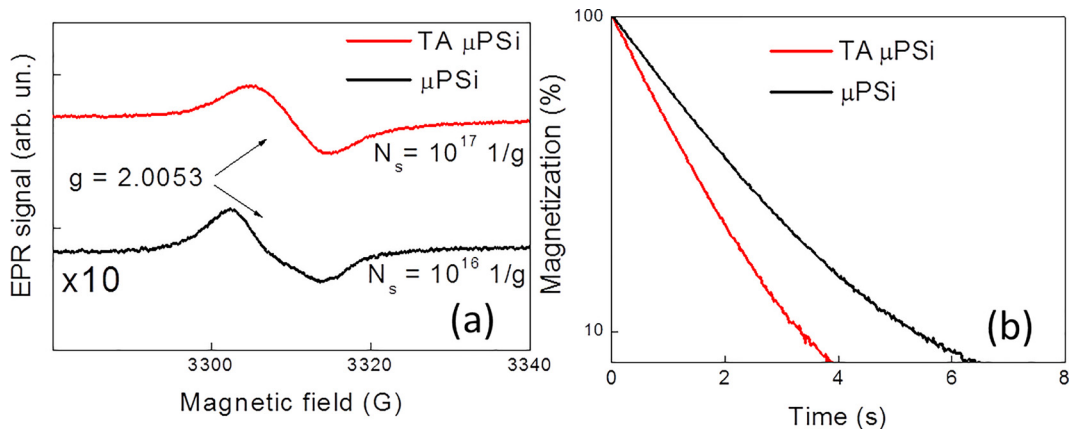


FIG. 5. (a) EPR spectra of as-prepared (black line, the intensity is multiplied by 10 times) and thermally annealed in vacuum (red line) μ PSi NPs. (b) Transients of the transverse proton magnetization in aqueous suspensions of as-prepared (black line) and thermally annealed in vacuum (red line) μ PSi NPs.

In order to decrease the concentration of Si DBs, we used MPSi NPs, which were thermally oxidized in air for 2 h at 300°C and then for 1 h at 900°C [thermally oxidized meso porous Si (TO MPSi)]. DLS spectra of the aqueous suspensions of TO MPSi NPs and FTIR spectra of the dried NPs are shown in Fig. 2S of [supplementary material](#). EPR spectra of MPSi NPs before (red curve) and after oxidation (blue curve) are shown in Fig. 6. The spectrum of TO MPSi was multiplied 10 times for visual convenience. After oxidation, the DBs concentration was decreased by 3 times due to their passivation by oxygen and the EPR signal markedly broadened and deviated from the Lorentz function.^{23,31,32} This fact is probably related to a superposition of different types of Pb centers contributing to the EPR signal.²⁹

The transverse relaxation rate, R_2 , which is induced by NPs, can be calculated according to the following equation:²¹

$$R_2 \equiv (T_2^{NP})^{-1} = (T_2)^{-1} - (T_2^W)^{-1}, \quad (1)$$

where T_2^{NP} is the effective time of transverse relaxation due to the presence of NPs, T_2 is measured transverse relaxation time for the NP suspension and T_2^W is the measured transverse relaxation time in pure water.

Figure 7 shows dependences of R_2 on concentration of MPSi NPs. The concentration dependences are nearly linear for both as-prepared and TO MPSi. This fact indicates that both types of NPs do not aggregate in concentrated suspensions and the pores are still open in the TO MPSi. Indeed, the latter NPs are characterized by nearly three times lower concentration of paramagnetic centers in comparison with the as-prepared ones (see Fig. 6) that causes 3 times lower R_2 in the whole range of the NP concentration (see Fig. 7).

It is known that CAs can be characterized by as-called relaxivity, which is defined as the change in relaxation rate after addition of CAs divided into the concentration of CAs.^{1,21,33} The value of r_2 for NPs can be expressed as follows:

$$r_2 = \frac{R_2}{C_{NP}}, \quad (2)$$

where R_2 is the proton relaxation rate governed by Si NPs, C_{NP} is the concentration of NPs in suspensions.

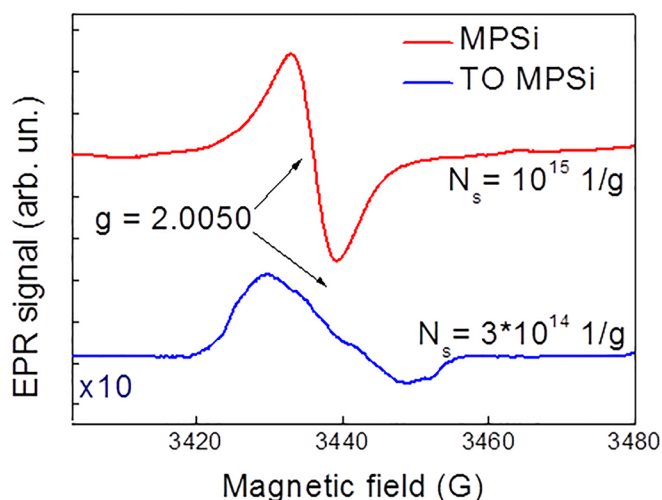


FIG. 6. EPR spectra of as-prepared (red line) and oxidized (blue line, the intensity is multiplied 10 times) MPSi NPs.

The data of Table I allow us to estimate the transverse relaxivity $r_2 \approx 0.5$ l/(g s) for TA μ PSi NPs, which possess the paramagnetic center concentration $\sim 10^{17}$ g $^{-1}$. One can also estimate the relaxivity divided on the average number of Si atom in NPs and it gives $r_2^{Si} \approx 10^{-2}$ l/(mmol s). The later value seems to be significantly smaller than that for conventional Gd $^{3+}$ and SPIO CAs, which are about 4–5.7 l/(mmol s) and 152–178 l/(mmol s).^{34–36} However, the relaxivity of Si-based NPs divided on the number of Si DBs is rather significant, i.e., $r_2^{DB} \approx 10^3$ l/(mmol s). Note that TA μ PSi NPs possessed approximately one DB per NP. This analysis indicates that Si NPs can be attractive CAs for biomedical application in MRI when they will possess largest amount of DBs, which will result in strongest enhancement of the transverse proton relaxation.

IV. CONCLUSIONS

The obtained experimental results confirm the role of Si dangling bonds in porous Si NPs for the enhancement of proton relaxation. The samples of nonporous crystalline Si NPs

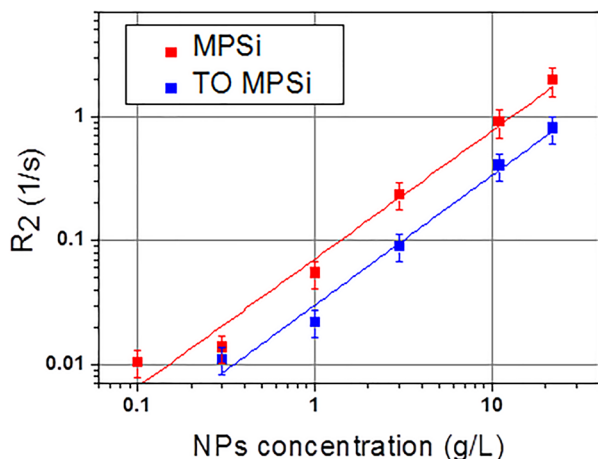


FIG. 7. Transverse relaxation rate R_2 of aqueous suspensions of as-prepared (red dots) and thermally oxidized in air MPSi NPs (blue dots) vs NPs concentration. Solid lines are linear fits.

exhibited the weak decrease of the both longitudinal and transverse relaxation times because of the low efficiency of the interaction of Si DBs in c-Si NPs with surrounding water molecules. On the one hand, thermally oxidized mesoporous Si NPs did not affect strongly the proton spin relaxation due to the low density of Si DBs. On the other hand, the microporous Si NPs thermally annealed in vacuum exhibited the strong decrease of the relaxation times, especially the transverse one. The transverse relaxation rate was found to depend almost linearly on the concentration of porous Si NPs in suspensions varied from 0.1 to 20 g/l. The relaxation rate induced by NPs was approximately proportional to the number of Si DBs on their surfaces, which ranged from 3×10^{14} to 10^{17} 1/g, indicating a way to enhance the proton relaxation. The transverse relaxivity of thermally annealed microporous Si NPs is estimated to be 0.5 l/(g s), which is already promising for MRI applications. The relaxivity of porous Si NPs can be additionally improved by using physical and chemical treatments, which will lead to increasing the number of paramagnetic centers in the NPs, ensuring further progress in the exploring of Si NPs as prospective contrast agents for MRI.

SUPPLEMENTARY MATERIAL

See [supplementary material](#), which consists of the experimental data on porous morphology and sizes of porous Si NPs (Fig. 1S), and characterization of thermally oxidized mesoporous Si NPs (Figs. 2S and 3S). The measured concentration dependence of the transverse relaxation rate of a Gd-based contrast agent (Magnevist) is shown in Fig. 4S.

ACKNOWLEDGMENTS

The authors are grateful to L. A. Osminkina and S. S. Abramchuk for their assistance in the sample preparation and TEM measurements, respectively. This work was partially supported by the Russian Foundation for Basic Research (Grant No. 16-02-00668). Yu.V.K. greatly acknowledges the financial support of the Foundation for the Promotion of Small Innovative Enterprises in the Scientific and Technical Sphere under the UMNiK program on the topic of “Development of magnetic resonance contrast agents based on silicon nanoparticles for tumors diagnosis” under the Contract No. 8982GU/2015. V.Yu.T. thanks the support of the Ministry of Education and Science of Russia (State Project No. 16.2969.2017/4.6).

¹G. J. Strijkers, W. J. M. Mulder, G. A. F. van Tilborg, and K. Nicolay, *Anticancer Agents Med. Chem.* **7**, 291 (2007).

²F. G. Shellock and E. Kanal, *J. Magn. Reson. Imaging* **10**, 477 (1999).

³H. S. Thomsen, S. K. Morcos, and P. Dawson, *Clin. Radiol.* **61**, 905 (2006).

⁴J.-M. Idee, M. Port, I. Raynal, M. Schaefer, S. Le Greneur, and C. Corot, *Fundam. Clin. Pharmacol.* **20**, 563 (2006).

⁵M. F. Bellin, M. Vasile, and S. Morel-Precetti, *Eur. Radiol.* **13**, 2688 (2003).

⁶M. Mahmoudi, H. Hofmann, B. Rothen-Rutishauser, and A. Petri-Fink, *Chem. Rev.* **112**, 2323 (2012).

⁷L. T. J. H. Park, L. Gu, G. von Maltzahn, E. Ruoslahti, S. N. Bhatia, and M. J. Sailor, *Nat. Mater.* **8**, 331 (2009).

- ⁸L. A. Osminkina, K. P. Tamarov, A. P. Sviridov, R. A. Galkin, M. B. Gongalsky, V. V. Solovyev, A. A. Kudryavtsev, and V. Y. Timoshenko, *J. Biophotonics* **5**(7), 529 (2012).
- ⁹A. P. Sviridov, L. A. Osminkina, A. Y. Kharin, M. B. Gongalsky, J. V. Kargina, A. A. Kudryavtsev, Y. I. Bezsudnova, T. S. Perova, A. Geloen, V. Lysenko, and V. Y. Timoshenko, *Nanotechnology* **28**, 105102 (2017).
- ¹⁰A. D. Durnev, A. S. Solomina, N. O. Daugel-Dauge, A. K. Zhanataev, E. D. Shreder, E. P. Nemova, O. V. Shreder, V. A. Veligura, L. A. Osminkina, and V. Y. Timoshenko, *Bull. Exp. Biol. Med.* **149**, 445 (2010).
- ¹¹S. Murugadoss, D. Lison, L. Godderis, S. Van Den Brule, J. Mast, F. Brassinne, N. Sebaihi, and P. H. Hoet, *Arch. Toxicol.* **91**, 2967 (2017).
- ¹²H. Bahadar, F. Maqbool, K. Niaz, and M. Abdollahi, *Iran Biomed. J.* **20**, 1 (2016).
- ¹³L. A. Osminkina, A. L. Nikolaev, A. P. Sviridov, N. V. Andronova, K. P. Tamarov, M. B. Gongalsky, A. A. Kudryavtsev, H. M. Treshalina, and V. Yu. Timoshenko, *Microporous Mesoporous Mater.* **210**, 169 (2015).
- ¹⁴L. Canham, *Nanotechnology* **18**, 185704 (2007).
- ¹⁵J. Salonen and V. P. Lehto, *Chem. Eng. J.* **137**, 162 (2008).
- ¹⁶L. Xiao, L. Gu, S. B. Howell, and M. J. Sailor, *ACS Nano* **5**, 3651 (2011).
- ¹⁷A. P. Sviridov, V. G. Andreev, E. M. Ivanova, L. A. Osminkina, K. P. Tamarov, and V. Y. Timoshenko, *Appl. Phys. Lett.* **103**, 193110 (2013).
- ¹⁸K. P. Tamarov, L. A. Osminkina, S. V. Zinovyev, K. A. Maximova, J. V. Kargina, M. B. Gongalsky, Y. V. Ryabchikov, A. Al-Kattan, A. P. Sviridov, M. Sentis, A. V. Ivanov, V. N. Nikiforov, A. V. Kabashin, and V. Y. Timoshenko, *Sci. Rep.* **4**, 7034 (2014).
- ¹⁹J. W. Apteekar, M. C. Cassidy, A. C. Johnson, R. A. Barton, M. Lee, A. C. Ogier, C. Vo, M. N. Anahar, Y. Ren, S. N. Bhatia, C. Ramanathan, D. G. Cory, A. L. Hill, R. W. Mair, M. S. Rosen, R. L. Walsworth, and C. M. Marcus, *ACS Nano* **3**, 4003 (2009).
- ²⁰F. Erogbogbo, C. W. Chang, J. L. May, L. Liu, R. Kumar, W. C. Law, H. Ding, K. T. Yong, I. Roy, M. Sheshadri, M. T. Swihart, and P. N. Prasad, *Nanoscale* **4**, 5483 (2012).
- ²¹M. B. Gongalsky, Y. V. Kargina, L. A. Osminkina, A. M. Perepukhov, M. V. Gulyaev, A. N. Vasiliev, Y. A. Pirogov, A. V. Maximychev, and V. Y. Timoshenko, *Appl. Phys. Lett.* **107**, 233702 (2015).
- ²²A. Perepukhov, O. Kishenkov, A. Maximychev, S. Gudenko, L. Menshikov, and D. Alexandrov, *Microporous Mesoporous Mater.* **205**, 7 (2015).
- ²³A. G. Cullis, L. T. Canham, and P. D. J. Calcott, *J. Appl. Phys.* **82**, 909 (1997).
- ²⁴L. A. Osminkina and V. Y. Timoshenko, *Mesoporous Biomater.* **3**, 39 (2016).
- ²⁵B. K. Meyer, D. M. Hofmann, W. Stadler, V. P. Koch, F. Koch, P. Omling, and P. Emanuelsson, *Appl. Phys. Lett.* **63**, 2120 (1993).
- ²⁶D. Pierreux and A. Stesmans, *Phys. Rev. B* **66**, 165320 (2002).
- ²⁷Y. Xiao, T. J. McMahon, J. I. Pankove, and Y. S. Tsuo, *J. Appl. Phys.* **76**, 1759 (1994).
- ²⁸J. L. Cantin, M. Schoisswohl, H. J. von Bardeleben, N. Hadj Zoubir, and M. Vergnat, *Phys. Rev. B* **52**, R11599(R) (1995).
- ²⁹H. J. von Bardeleben, D. Stievenard, A. Grosman, C. Ortega, and J. Siejka, *Phys. Rev. B* **47**, 10899 (1993).
- ³⁰R. N. Pereira, S. Niesar, H. Wiggers, M. S. Brandt, and M. S. Stutzmann, *Phys. Rev. B* **88**, 155430 (2013).
- ³¹A. Pavlikov, E. Konstantinova, and V. Timoshenko, *Phys. Status Solidi C* **8**, 1928 (2011).
- ³²B. K. Meyer, V. Petrova Koch, T. Muschik, H. Linke, P. Omling *et al.*, *Appl. Phys. Lett.* **63**, 1930 (1993).
- ³³R. B. Lauffer, *Chem. Rev.* **87**, 901 (1987).
- ³⁴H. J. Weinmann, R. C. Brasch, W. R. Press, and G. E. Wesbey, *Am. J. Roentgenol.* **142**, 619 (1984).
- ³⁵M. Rohrer, H. Bauer, J. Mintorovitch, M. Requardt, and H.-J. Weinmann, *Invest. Radiol.* **40**, 715 (2005).
- ³⁶M. K. Uchiyama, S. H. Toma, S. F. Rodrigues, A. L. Borges Shimada, R. A. Loiola, H. J. Cervantes Rodríguez, P. V. Oliveira, M. S. Luz, S. R. Rabbani, H. E. Toma, S. H. Poliselli Farsky, and K. Araki, *Int. J. Nanomed.* **10**, 4731 (2015).